

# Reinterpretation of the Expected Electronic Density of States of Semiconductor Nanowires

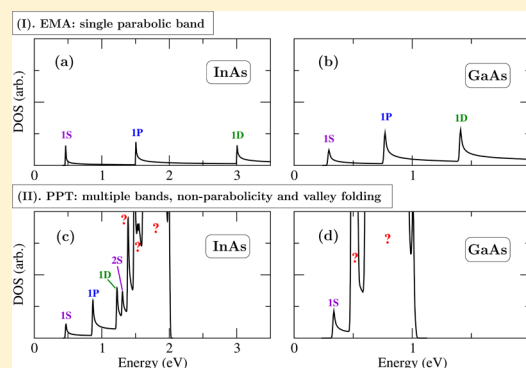
Jianping Wang,<sup>†,§</sup> Jun-Wei Luo,<sup>‡,||</sup> Lijun Zhang,<sup>\*,†,⊥</sup> and Alex Zunger<sup>\*,†</sup>

<sup>†</sup>University of Colorado, Boulder, Colorado 80309, United States

<sup>‡</sup>National Renewable Energy Laboratory, Golden, Colorado 80401, United States

**ABSTRACT:** One-dimensional semiconductor nanowires hold the promise for various optoelectronic applications since they combine the advantages of quantized in-plane energy levels (as in zero-dimensional quantum dots) with a continuous energy spectrum along the growth direction (as in three-dimensional bulk materials). This dual characteristic is reflected in the density of states (DOS), which is thus the key quantity describing the electronic structures of nanowires, central to the analysis of electronic transport and spectroscopy. By comparing the DOS derived from the widely used “standard model”, the effective mass approximation (EMA) in single parabolic band mode, with that from direct atomistic pseudopotential theory calculations for GaAs and InAs nanowires, we uncover significant qualitative and quantitative shortcomings of the standard description. In the EMA description the nanowire DOS is rendered as a series of sharply rising peaks having slowly decaying tails, with characteristic peak height and spacing, all being classifiable in the language of atomic orbital momenta 1S, 1P, 1D, etc. Herein we find in the thinner nanowires that the picture changes significantly in that not only does the profile of each DOS peak lose its pronounced asymmetry, with significant changes in peak width, height, and spacing, but also the origin of the high-energy peaks changes fundamentally: below some critical diameter, the region of atomic orbital momentum classified states is occupied by a new set of DOS peaks folded-in from other non- $\Gamma$ -valleys. We describe explicitly how distinct physical effects beyond the conventional EMA model contribute to these realistic DOS features. These results represent a significant step toward understanding the intriguing electronic structure of nanowires reflecting the coexistence of discrete and continuum states. Experimental examinations of the predicted novel DOS features are called for.

**KEYWORDS:** Nanowires, density of states, quantum confinement, semiconductor



Semiconductor nanowires are featured prominently as candidates for many electronic and optical device applications such as nanotransistors,<sup>1,2</sup> nanolasers,<sup>3–5</sup> thermoelectrics,<sup>6,7</sup> and solar energy harvesting,<sup>8–12</sup> and facilitate fundamental science innovations such as detection of Majorana fermions<sup>13,14</sup> and realization of one-dimensional (1D) heterojunctions.<sup>15,16</sup> Unlike the case of zero-dimensional (0D) quantum dots, which are characterized by discrete energy levels as the result of quantum confinement effect, 1D nanowires simultaneously have an in-plane quantized energy levels and a continuous energy spectrum due to periodicity along the growth direction, so the central quantity used to characterize their electronic structure is the density of states (DOS). The nanowire DOS can be measured by scanning tunneling spectroscopy,<sup>17,18</sup> X-ray absorption spectroscopy,<sup>19</sup> Kelvin probe force microscopy,<sup>20</sup> and also indirectly derived from transport related quantities such as conductance<sup>13,21</sup> and thermopower.<sup>22</sup> Knowledge of the nanowire DOS is important for analyzing the properties relevant to band filling of carriers, e.g., electron transport under external fields,<sup>23</sup> hot carrier excitation and relaxation at high temperatures.<sup>24</sup> Although quantitative experimental measurements of semiconductor

nanowire DOS are not yet advanced to the point of direct comparison with theory, the discussion of the differences between expectations based on different levels of theoretical approach is not premature.

Traditionally, the DOS of nanowires has been formulated and taught in terms of the effective mass approximation (EMA),<sup>25</sup> where a single parabolic band of the  $\Gamma$ -valley is assumed. The idea is to describe a nanostructure in the language of the three-dimensional (3D) bulk material from which it is drawn, rather than a large molecule in its own right. The DOS of conduction bands calculated with this approach is illustrated in part I of Figure 1 (Figure 1a for InAs nanowires and Figure 1b for GaAs nanowires). As seen, the EMA rendering of nanowire DOS has the following features: (i) it can be well classified into the peaks associated with the angular momentum states (of the orbital momenta of 1S, 1P, 1D, etc.) with quantized sub-band energy levels  $E_{\text{sub}}$  within the confined plane (perpendicular to the growth direction). (ii) Each peak

**Received:** August 5, 2014

**Revised:** November 16, 2014

**Published:** November 30, 2014

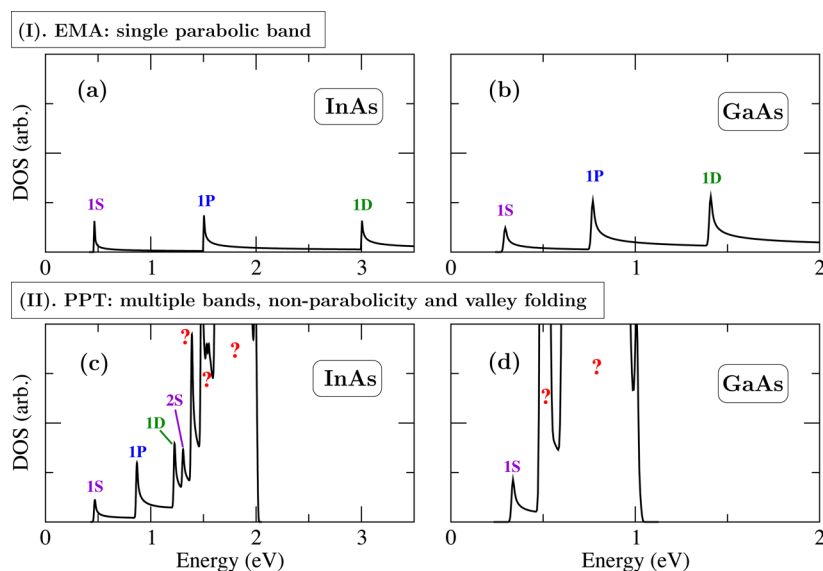


**Figure 1.** DOS of conduction bands for InAs (a,c) and GaAs (b,d) nanowires at the diameter of 5 nm calculated with the EMA (I, upper panels) and the PPT (II, lower panels). All the nanowires are built from the zinc blende structure, oriented along the [111] direction and passivated by a surrounding generic barrier material. The orbital momenta of identified peaks are labeled (S in purple, P in blue, and D in green). In the part II for those peaks without any angular momentum feature, the question marks (in red) are placed. Note that for the same material (a and c, or b and d) the scales of both  $x$ -axis and  $y$ -axis are the same.

shows a sharp energy rise at  $E_{\text{sub}}$  and long tail of slow energy decay (in the form of  $1/\sqrt{E - E_{\text{sub}}}$ , where  $E$  is energy). (iii) The peak heights of doubly degenerate 1P and 1D states are higher than that of the 1S state with single degeneracy. (iv) Complying with quantum confinement effect,  $E_{\text{sub}}$  scales as  $1/m^*d^2$ , where  $m^*$  is electron effective mass and  $d$  is nanowire diameter. So at the same  $d$ , for InAs (Figure 1a) with the smaller effective mass ( $0.024m_0$  compared with  $0.068m_0$  of GaAs), the energy distances among different DOS peaks are larger. The features (i)–(iv) are standard expectations for the shape and form of the nanowire DOS in typical semiconductors.

Since in the EMA a nanostructure is described straightforwardly by the band parameters of 3D bulk material, it is perhaps not surprising that the EMA rendering of electronic states may be rather approximate, given the disparity between the 3D bulk reference and the lower-dimensional confined system being described. Differences between the EMA and direct atomistic pseudopotential theory (PPT) calculations<sup>26–28</sup> for 0D quantum dots were described previously and include the fact that both valence and conduction bands derived from the EMA miss many states present in the direct calculations<sup>29–31</sup> and even the orbital symmetries of some states are often misrepresented.<sup>32,33</sup> Since the disparity between the 3D bulk reference and the 1D nanowire is smaller than that in the case of 0D quantum dots, it would be interesting to examine the validity of the EMA description of the nanowire electronic structure relative to the descriptions free from the approximations underlying it. With this motivation, we have recently extended our PPT calculations of the electronic structure of nanostructures from 0D quantum dots to 1D nanowires.<sup>34–36</sup> The ensuing nanowire DOS of conduction bands calculated by the PPT (part II of Figure 1) for InAs and GaAs are shown in Figure 1c,d respectively, where they are compared with the EMA DOS (part I of Figure 1) of the same material, same diameter, and same passivation. Significant differences are apparent between the EMA and the atomistic

PPT calculations, including (i) the atomistically described DOS is deformed significantly toward the lower energy side. In particular, for the InAs nanowire (Figure 1c), while the 1S peak does not show much change, remarkable blue shift occurs to the 1P and 1D peaks, and meanwhile, the higher-energy excited 2S state appears in the energy window shown. (ii) In addition to the change of energy position, the width of each DOS peak decreases and the long tails with slow energy decay disappear. (iii) The heights of the peaks are enhanced as the result of the disappearance of long tails and the overlap between adjacent peaks. (iv) Additional DOS peaks (labeled by the question mark, to be explained below), which cannot be attributed to any angular momentum state of the  $\Gamma$ -valley, emerge in the higher-energy side of Figure 1c,d. With these unambiguous differences, it is clear that the textbook description in the framework of EMA for nanowire DOS is a rather coarse model, missing many qualitative as well as quantitative aspects of DOS features. Yet, the DOS is an important quantity in modern nanowire science, used very often for discussing and interpreting experimental measurements;<sup>21,22</sup> its qualitative misrepresentation might affect in a negative way the interpretation of the physical mechanism relevant to DOS features.

In this letter we uncover significant qualitative and quantitative shortcomings of the standard model describing the nanowire DOS based on the EMA. We will clarify by treating one effect at the time what are the physical factors that control the differences between the parts I and II of Figure 1, i.e., the significant deformation of realistic DOS away from the standard EMA model. We will focus on the DOS of electrons (conduction bands) being more relevant to experimental interests in semiconductor nanowires, but similar principles can be adapted to holes (valence bands). This work provides a useful insight into accurate description of the nanowire DOS, offering a useful foundation to correctly understanding relevant experimental observations.

**Sequential Introduction of Different Physical Factors Considered Step-by-Step in the Nanowire DOS Calculations.** The approaches we took are stepwise, treating one effect at the time, so as to address different aspects of physical effects controlling the nanowire DOS. Briefly the following four levels of methodology from simple to complex are employed:

A. First, we start with the EMA, the model of single parabolic band (without nonparabolicity and interband coupling), assuming finite potential barrier, but the same effective mass in nanowire and its environment. Here, the electronic structure of nanowires is calculated by solving the Schrödinger eqs 1 and 2 for an infinite cylinder along the  $z$  (nanowire growth) direction with the diameter  $R$ , surrounded by the barrier with the potential height  $V_0$ <sup>25</sup>

$$\left[ -\frac{\hbar^2}{2m^*} \left( \frac{1}{r} \frac{d}{dr} r \frac{d}{dr} + \frac{1}{r^2} \frac{d^2}{d\varphi^2} + \frac{d^2}{dz^2} \right) \right] \psi_w(\vec{r}) = E \psi_w(\vec{r}), \quad (1)$$

$$r < R$$

$$\left[ -\frac{\hbar^2}{2m^*} \left( \frac{1}{r} \frac{d}{dr} r \frac{d}{dr} + \frac{1}{r^2} \frac{d^2}{d\varphi^2} + \frac{d^2}{dz^2} \right) \right] \psi_b(\vec{r}) = (E - V_0) \psi_b(\vec{r}), \quad r > R \quad (2)$$

where  $m^*$  is the electron effective mass. The wave function of nanowire  $\psi_w(\vec{r})$  and barrier  $\psi_b(\vec{r})$  comply with the boundary condition of  $\psi_w(\vec{r})_{r=R} = \psi_b(\vec{r})_{r=R}$  by which the in-plane quantum confinement effect is enforced. In this model the only material dependent parameter is  $m^*$ , which is taken from the assumed parabolic band of bulk material. The bulk effective mass  $m^*$  ( $0.024m_0$  for InAs and  $0.068m_0$  for GaAs) is used, and the same potential height  $V_0$  as that of the atomistic PPT calculation (4.6 eV for InAs and 3.5 eV for GaAs) is chosen for direct comparison (as in Figure 1).

B. Second, we allow different effective masses of the nanowire and its environment. In step A, the effective mass  $m^*$  is taken as a constant across the nanowire and surrounding materials outside. This is, however, not reflecting the actual fact that semiconductor nanowires are passivated by either organic ligands or embedded in some shell materials during their growth.<sup>37</sup> To reasonably acknowledge this fact, in this step we allow an effective mass discontinuity, i.e., by making the effective masses of nanowire (in eq 1) and surrounding barrier (in eq 2) different. This is done by adding into the EMA of step A the BenDaniel–Duke boundary condition  $1/m_w^* \nabla \psi_w(\vec{r})_{r=R} = 1/m_b^* \nabla \psi_b(\vec{r})_{r=R}$ ,<sup>38</sup> where  $m_w^*$  and  $m_b^*$  represent the effective mass of nanowire and barrier, respectively. Then we can systematically vary the ratio between  $m_w^*$  and  $m_b^*$  to explore the effect of effective mass discontinuity on the nanowire DOS.

C. Next, we allow the bulk band structure exhibiting nonparabolicity, still without interband coupling. In most semiconductors, as the result of band-mixing effects, the realistic band structure usually deviates from the parabolic shape, especially at the  $k$ -points away from  $\Gamma$  and on the way to the Brillouin zone boundary.<sup>39</sup> To properly include the effect of band nonparabolicity, we employed the single-band truncated crystal (SBTC) approach.<sup>40–42</sup> It entails two steps: (i) first, a realistic dispersion of the 3D bulk conduction band is accounted for, including all the nonparabolic features, as obtained from the accurate band structure of bulk material; here, we use the PPT<sup>26–28</sup> for band structure calculations (but

any other accurate electronic structure method will fit the purpose). (ii) Then, the in-plane quantized sub-band energy levels  $E_{\text{sub}}$  is evaluated by determining the wave vectors  $\{k\}$  within the bulk band structure at which the nanowire carved out of the bulk has wave functions vanishing at the boundary (by assuming an infinite potential barrier surrounding the nanowire). This approach retains kinetic energy controlled quantum confinement effect, but deliberately neglects the coupling among multiple bands (by using precisely bulk eigenstates).

D. Finally we allow all the effects in A, B, and C, plus the effect of band coupling and valley folding. This is done by employing the PPT, a fully atomistic quantum-mechanical calculation where the electronic structure of nanowires is obtained by solving the semiempirical single-particle Schrödinger equation:

$$\left[ -\frac{\hbar^2}{2m} \nabla^2 + V_{\text{loc}}(\mathbf{r}) + \hat{V}_{\text{SO}} \right] \psi_i(\mathbf{r}) = \epsilon_i \psi_i(\mathbf{r}) \quad (3)$$

where  $\hat{V}_{\text{SO}}$  is the nonlocal spin–orbit operator, and  $V_{\text{loc}}(\mathbf{r})$  is the local potential that is given by the superposition of screened atomic pseudopotentials centered at the atomic positions  $\{\mathbf{R}_n\}$ :  $V_{\text{loc}}(\mathbf{r}) = \sum_n v_n(|\mathbf{r} - \mathbf{R}_n|)$ . Unlike the classic empirical pseudopotential method,<sup>43</sup> the atomic pseudopotentials in our PPT approach are fitted to accurately reproduce a wide range of critical parameters of band structure, e.g., transition energies, deformation potential, effective masses, spin–orbit couplings, etc., as determined by ab initio calculations.<sup>26–28,44</sup>

The PPT approach overcomes in a practical way the well-known issue in the density functional theory calculations, i.e., seriously underestimating the band gap, as well as effective mass (band dispersion), thus suitable for the current nanowire DOS study. The nanowires adopt the zinc blende crystalline structure. The barrier material surrounding the nanowire is not a set of organic ligands but actually modeled as an interfacial heterostructure between a nanowire and its surrounding environment. This passivating barrier material is modeled by a pseudopotential that has the same structure as the nanowire material but presents band offsets  $\Delta E_C$  and  $\Delta E_V$  with the conduction and valence band edges of nanowire, respectively. The pseudopotential describing the barrier material is selected to mimic an oxide with a large band gap of the order of 8 eV and a conduction band offset of  $\Delta E_C \approx 4$  eV and  $\Delta E_V \approx 3$  eV. The large band gap of the barrier material corresponds to a 5–10 times heavier (than that of nanowire material) effective mass of electron  $m^* \approx 0.3m_0$ . The barrier is extended spatially to the edges of the periodic supercell. The main DOS features shown in part II of Figure 1 are not sensitive to the magnitude of the confining band offset  $\Delta E_C$ . This passivation completely eliminates dangling bonds residing on the nanowire surface. No calculation is conducted for the bare or less passivated nanowire since the entailed dangling bonds will cause the midgap electronic states, acting as nonradiative recombination centers. Equation 3 is diagonalized within a plane-wave basis, and the eigensolutions are calculated using the folded-spectrum method,<sup>45</sup> which has a computational cost that scales linearly with the number of atoms in the system. By capturing the realistic atomistic morphology of nanostructures and solving the quantum mechanical eq 3, this approach naturally includes all the factors missing in the EMA of step A, e.g., the effect of effective mass discontinuity (step B), band nonparabolicity (step C), and band coupling (among

conduction bands, as well as between conduction and valence bands) as the result of the removal of translation symmetry and other symmetry breaking in nanostructures,<sup>46,47</sup> as well as the band folding originated from the higher energy valleys at the symmetry points of Brillouin zone other than  $\Gamma$  (to be discussed in detail below).

**Selection of Semiconductors Composing Nanowires To Be Studied.** In principle the approaches above can be applied to any semiconductor nanowires. First, in order to highlight the effect of nonparabolicity (the above step C), we select InAs as one of the materials composing nanowires since it has a conduction band with rather large nonparabolicity.<sup>48</sup> Second, to illustrate clearly the effects of band coupling and valley folding (step D) we aimed at choosing a material that has energetically close competing conduction band valleys (at  $\Gamma$  and non- $\Gamma$   $k$ -points). In the nanowires made from the material with the non- $\Gamma$ -valleys close in energy to the  $\Gamma$  one, the non- $\Gamma$ -valleys will be folded to the energy region in proximity to (or overlapping with) the  $\Gamma$ -valley derived states, coupling strongly with them and also contributing directly to the DOS profile. By considering this, we selected GaAs as another constituted material, which has the relatively small energy distance between X- and  $\Gamma$ -valleys (0.30 eV compared with 1.02 eV of InAs) and also between L- and  $\Gamma$ -valleys (0.46 eV compared with 0.72 eV of InAs). Finally, we note that since common organic ligands passivating nanowire surfaces give rise to molecular energy levels, which resemble the materials with extremely large effective masses, resulting in significant effective mass discontinuity between  $m_w^*$  and  $m_b^*$  (step B). To mimic this fact, the effective mass of barrier  $m_b^*$  is chosen to be  $\sim 0.3m_0$ , which is 5–10 times larger than that of selected InAs ( $0.024m_0$ ) or GaAs ( $0.068m_0$ ) making up nanowires. All the nanowires involved in this work are constructed as the infinite cylinders from the zinc blende structure, oriented along the [111] direction, which is the predominant growth direction thermodynamically favored in experiments.<sup>37</sup> At the diameter of 5 nm (the one we focus on here), the nanowire contains about 130 atoms in the cross-section plane.

**Effect of Effective Mass Discontinuity on the Nanowire DOS.** As schematically shown in Figure 2a, we built nanowires (with the effective mass  $m_w^*$ ) surrounded by passivation barriers with a different effective mass  $m_b^*$  and performed the DOS calculations at different ratios between  $m_w^*$  and  $m_b^*$  (see the above step B). Figure 2b shows the resulted DOS of InAs nanowires ( $d = 5$  nm) for  $m_b^*/m_w^* = 11.7$  (upper panel) and the constant effective mass case,  $m_b^*/m_w^* = 1.0$  (lower panel, the above step A). As seen, while the general shape of DOS peaks did not change, the larger value of  $m_b^*/m_w^*$  leads to remarkable energy red-shift of all the peaks. The amount of shift increases with the atomic orbital momentum, and for the higher momentum 1P and 1D states, the shifts reach  $\sim 1$  eV. This implies the larger effective mass of barrier  $m_b^*$  has an equivalent effect of significantly weakening quantum confinement in nanowires. It is hence of great necessity to include this effective mass discontinuity in the nanowire DOS calculations.

**Effect of Band Nonparabolicity of Bulk Material on the Nanowire DOS.** In semiconductor nanowires, the nonparabolicity features of bands can be classified into two types in terms of their effects on electronic structure of 1D system: the in-plane nonparabolicity and the out-of-plane (along the growth direction) nonparabolicity. We probed the effect of in-plane nonparabolicity on the nanowire DOS via the

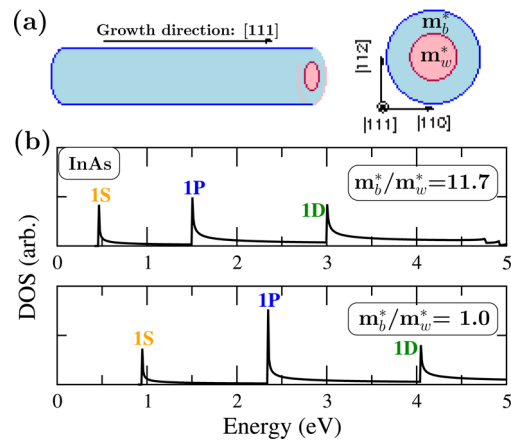


**Figure 2.** (a) Schematic plot of the [111]-oriented nanowire surrounded by the passivation barrier (left panel) and the sectional view (right panel). The nanowire and the barrier have different effective masses (denoted as  $m_w^*$  and  $m_b^*$ , respectively). (b) Calculated DOS of conduction bands for InAs nanowire ( $d = 5$  nm) with different values of  $m_b^*/m_w^*$ , i.e., 11.7 (upper panel) and 1.0 (lower panel) by using the EMA plus the BenDaniel–Duke boundary condition.

SBTC approach (see the above step C). Figure 3c shows the SBTC rendered quantized sub-band energy levels  $E_{\text{sub}}$  at the

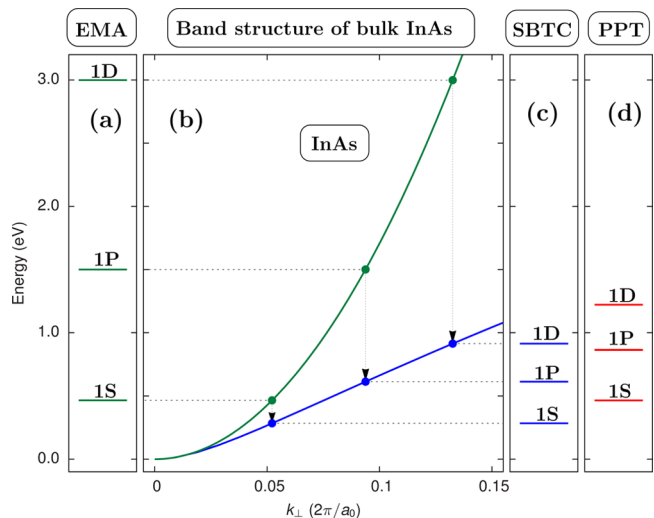


**Figure 3.** Quantized sub-band energy levels  $E_{\text{sub}}$  of 1S, 1P, and 1D conduction states at the zone center for the InAs nanowire ( $d = 5$  nm) evaluated via (a) the EMA, (c) the SBTC, and (d) the PPT. The purpose of plot (b) is to show how  $E_{\text{sub}}$  in (a) and (c) are evaluated by mapping onto corresponding bulk band dispersion in the spirit of SBTC (see text). The energy is given with respect to the CBM of bulk InAs. The effective masses (of nanowire and barrier) and potential height of barrier are the same in (a), (c), and (d).

zone center for InAs nanowire ( $d = 5$  nm), compared with those from the EMA (Figure 3a). Figure 3b shows how the sub-band energy levels  $E_{\text{sub}}$  in Figure 3c,a are evaluated via mapping onto corresponding band dispersion of bulk InAs. It is clearly seen that the in-plane nonparabolicity results in significantly decreased  $E_{\text{sub}}$  of all the 1S, 1P, and 1D states, making them bunched toward the lower-energy side. The higher atomic orbital momentum of the state, the larger red-shift of energy level is observed; for the 1D state, the energy shift is as large as  $\sim 2$  eV. Figure 4b shows the DOS of the first 1S state for the

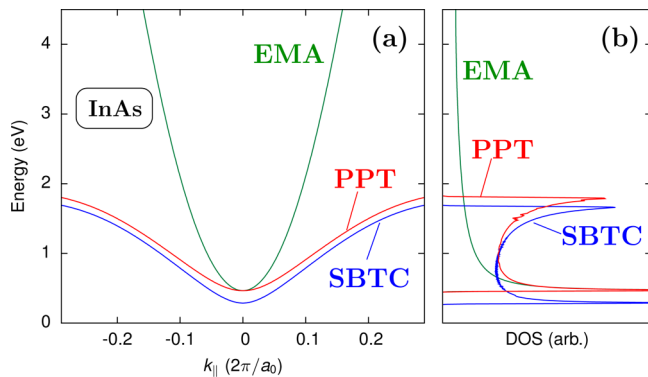


**Figure 4.** (a) Calculated band structure and (b) corresponding DOS for the first 1S conduction state of InAs nanowire ( $d = 5$  nm) by using the EMA (green), the SBTC (blue), and the PPT (red), respectively. The energy is given relative to the CBM of bulk InAs. For these calculations involving the single band, the DOS has been renormalized to guarantee the integration equal to 1.

same nanowire by using different approaches. As expected, the ensuing DOS peak from the SBTC (the first peak in blue below 0.5 eV) exhibits a red-shift by comparison with that from the EMA (the peak in green).

Turning to the out-of-plane nonparabolicity, its effect on the nanowire DOS is reflected directly by the nanowire band dispersion (of the 1S state) along the growth direction as shown in Figure 4a. We can see that compared with the band dispersion from the EMA (the green band), the nonparabolicity (represented by the blue band of SBTC) causes a rather heavier

band with less dispersion. This gives rise to two aspects of effects on the nanowire DOS, as shown in Figure 4b (the nonparabolicity of SBTC in blue and EMA in green): (i) it leads to the narrower DOS peak (i.e., the first peak in blue below 0.5 eV) and the long tail from EMA has been eliminated. (ii) Resulting from the very dispersiveless feature of band at the nanowire zone boundary (see the blue band in Figure 4a), a second peak at the higher energy emerges between 1.0 and 2.0 eV. These results indicate that in addition to the rigid shift of DOS peaks (via the effect of in-plane component), the nonparabolicity also plays an important role in changing the DOS shape and profile (due to the out-of-plane component).

#### Effect of Nanowire Interband Coupling on Its DOS.

We next explored the band coupling effect (resulting from the symmetry lowering in nanostructures) on the nanowire DOS. This can be straightforwardly extracted from the difference between the SBTC results (band coupling excluded) and the PPT calculations (band coupling included, see the above step D). The quantized sub-band energy levels  $E_{\text{sub}}$  for InAs nanowire ( $d = 5$  nm) are shown in Figure 3c (SBTC) and d (PPT), and the band dispersion of the 1S state and corresponding DOS are shown in Figure 4a,b (SBTC in blue and PPT in red), respectively. As seen, the predominant effect of band coupling is rigidly pushing  $E_{\text{sub}}$  and corresponding DOS peaks to the slightly higher energy region. This is the result of the competition between the coupling among conduction bands and that between conduction and valence bands.<sup>46,47</sup>

**Effect of Band Folding from Non- $\Gamma$ -Valleys on the Nanowire DOS.** In Figure 3d, we show only the PPT results of

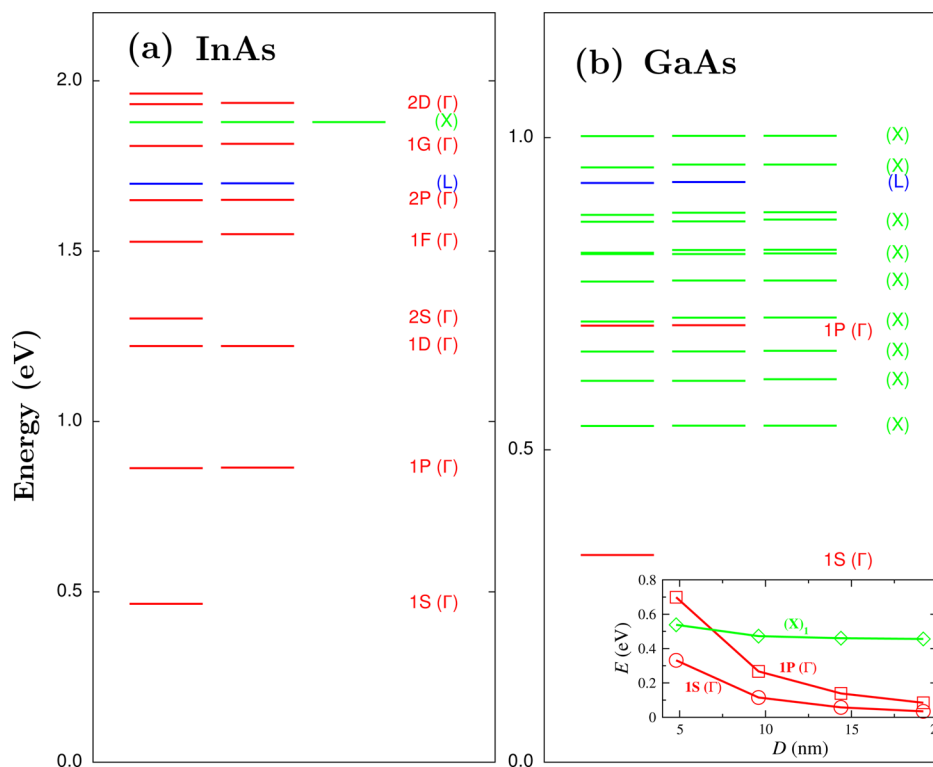


**Figure 5.** Complete quantized sub-band energy levels  $E_{\text{sub}}$  of conduction states at the zone center for the InAs (a) and GaAs (b) nanowires ( $d = 5$  nm) calculated with the PPT. The energy is relative to the CBM of corresponding bulk material. The valley origin of each electronic state ( $\Gamma$ -derived in red, L in blue, and X in green) and the shell-like orbital momenta (for  $\Gamma$ -valley derived states) are labeled. Multiple lines at the same energy level represent the degeneracy of states. For the GaAs nanowire, the diameter dependence of energy levels of 1S ( $\Gamma$ ), 1P ( $\Gamma$ ), and the first X-valley derived state ( $(X)_1$ ) is shown in the inset.

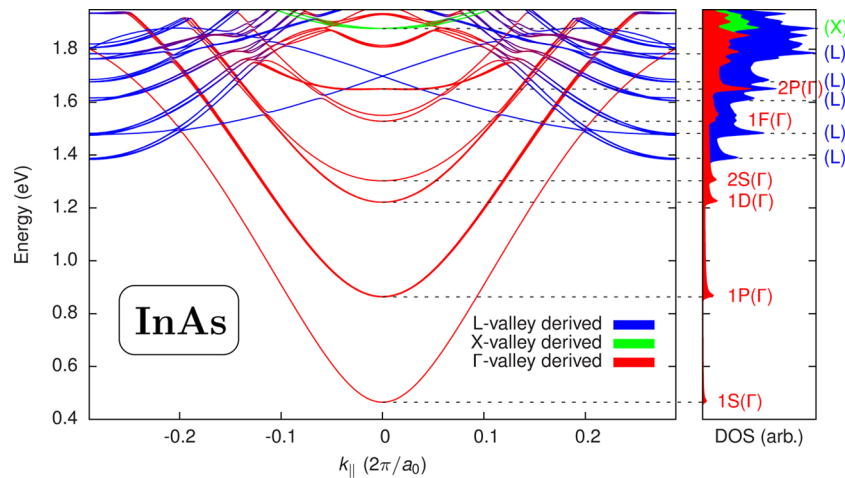


**Figure 6.** Calculated band structure (left panel) and DOS (right panel) of conduction bands for InAs nanowire ( $d = 5$  nm) by using the PPT. The energy is relative to the CBM of bulk InAs. For the left panel, different colors represent the valley origins of various electronic states ( $\Gamma$ , red; L, blue; X, green). Correspondingly, in the right panel the total DOS is decomposed into the contributions from different valley states.

the 1S, 1P, and 1D states originating from  $\Gamma$ -valley for clear comparison with the SBTC results. Actually there are more states appearing in the PPT calculations. Figure 5 shows the complete quantized sub-band energy levels  $E_{\text{sub}}$  for InAs and GaAs nanowire with  $d = 5$  nm. In terms of the band-folding picture for finite-size nanostructures, all the states can in principle be attributed to the lower-energy valley states at different  $k$ -points of the Brillouin zone in bulk band structure. We identified the valley origin of these states by using the majority representation approach,<sup>49</sup> i.e., by projecting their wave functions onto the complete bulk Bloch states at various  $k$ -points. In Figure 5 the valley origin of each state is labeled and its degeneracy is represented by the multiple lines at the same energy level. One immediately observes that in addition to the  $\Gamma$ -valley derived states (in red), there appear more states originating from the X-valley (in green) and L-valley (in blue). Particularly, in InAs nanowires (Figure 5a), two non- $\Gamma$ -valley states appear in the energy window shown, and the first L-valley state is located at  $\sim 1.7$  eV (above the  $\Gamma$ -valley 2P state). As to GaAs nanowire, a large number of X-valley states emerge and the first one starts from  $\sim 0.6$  eV; the only state below it is the  $\Gamma$ -valley 1S state. The remarkable distinction between InAs and GaAs nanowires is attributed to the energetically close competing conduction valleys of bulk GaAs as mentioned. Note that for the non- $\Gamma$ -valley states, the degeneracy is always higher than one (e.g., 3 for the X-valley state), as there are multiple valleys folded to the zone center of nanowires simultaneously.

Figures 6 and 7 show the PPT rendered band structure (left panel) and DOS (right panel) for InAs and GaAs nanowires at  $d = 5$  nm. The electronic states have been classified in terms of the origin from  $\Gamma$ -valley (red), L-valley (blue), or X-valley (green), respectively. Consistent with Figure 5, we can clearly see substantial contributions from the L-valley and X-valley derived states for both materials. Specifically, for InAs nanowire (Figure 6), in spite of the only one L-valley state existing at the zone center (at  $\sim 1.7$  eV), there appear a bunch of L-valley derived bands in proximity to the zone boundary, and thus, quite a number of associated DOS peaks with high intensity emerge above 1.3 eV. As to GaAs nanowire (Figure 7), the whole DOS has been predominantly occupied by the L-valley

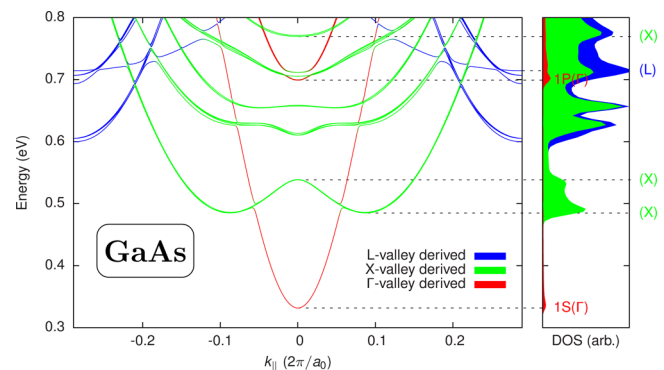


**Figure 7.** Calculated band structure (left panel) and DOS (right panel) of conduction bands for GaAs nanowire ( $d = 5$  nm) by using the PPT. The energy is relative to the CBM of bulk GaAs.

and X-valley derived states, and there exists only a very small portion of  $\Gamma$ -valley derived peaks.

**Dependence of Novel DOS Features Observed on the Nanowire Diameter.** We should point out that the roles of the above factors in affecting the nanowire DOS depend strongly on the degree of quantum confinement, which is determined by the nanowire diameter. For instance, it is known that for the most semiconductors serious deviation from the parabolic band shape usually occurs at the  $k$ -points away from  $\Gamma$  and on the way to the Brillouin zone boundary.<sup>39</sup> According to the band-folding picture, in wide nanowires the low-lying quantized energy levels derive from the states in proximity to the  $\Gamma$ -valley, but this is not the case in the thinner nanowires, where the states further away from the  $\Gamma$ -valley are involved. Hence for the fixed semiconductor material, the effect of nonparabolicity is more pronounced in the thinner nanowires made from it. Another factor closely related to the diameter is the band folding from the non- $\Gamma$ -valleys. In the nanowires with the smaller diameters, the increased quantum confinement will push the  $\Gamma$ -valley derived states (usually having the smaller  $m^*$  for electrons) to the higher excited-energy region. This gives the opportunity for the folded-in states from the non- $\Gamma$ -valleys (usually with heavy  $m^*$  and not quite sensitive to confinement) to emerge as the relatively low-lying excited states contributing to the DOS. In this work, in order to zoom in on the distinct

DOS features between the standard EMA model and the realistic case, we choose the thinner nanowires with the diameter of 5 nm. Actually the nanowires below this size have well reached the capability of modern nanowire growth,<sup>17,37</sup> and such small diameter nanowires accompanying with strong quantum confinement are of great interest to the application in nanoscale devices.<sup>50</sup> The inset of Figure 5b shows the calculated energy levels at the zone center of 1S ( $\Gamma$ ), 1P ( $\Gamma$ ), and the first X-valley derived state ( $(X)_1$ ) for the GaAs nanowire ranging from 5 to 20 nm. The X-valley derived state exhibits relatively weak dependence on quantum confinement owing to its heavy effective mass. The energy difference between  $(X)_1$  and 1P ( $\Gamma$ ) is  $-0.16$  eV at 5 nm,  $0.21$  eV at 10 nm,  $0.32$  eV at 15 nm, and  $0.37$  eV at 20 nm, respectively. Moreover, as shown in Figures 6 and 7 because of the band dispersion of the non- $\Gamma$ -valley derived states, their actual DOS peaks can extend into the region of the much lower energy. These imply that the novel DOS features we got here will be observable in the nanowires with large diameters that are achievable in current experimental nanowire growth.

**Conclusions.** We presented via fully quantum mechanical atomistic pseudopotential theory (PPT) calculations a systematic ab initio study of the density of states (DOS) of semiconductor nanowires, which controls the peculiar electronic structure combining discrete energy levels and continuous energy spectrum in the one-dimensional quantum system. Taking GaAs and InAs nanowires as examples, we find that while the conventional and widely used model based on effective mass approximation (EMA) may hold approximately for wide nanowires, it loses entirely its validity in the thinner nanowires by missing many qualitative as well as quantitative aspects of DOS features. This is unambiguously evidenced by direct comparison between the conventional EMA model and the realistic DOS from PPT calculations, where the realistic DOS shows not only significant change of DOS profile including peak spacing, width, and height but also unexpected emergence of new peaks originating from the folded-in states of non- $\Gamma$ -valleys. We explained explicitly how a variety of important physical factors contribute to the remarkable deformation of the realistic nanowire DOS away from the conventional model. These include effective mass discontinuity between nanowire and its environment, nonparabolicity of bands, coupling among multiple bands, and band folding from the non- $\Gamma$ -valleys. This work raises a warning flag when one attempts to interpret experimental data of transport and spectroscopy by using the conventional EMA model of the nanowire DOS. Its oversimplified form with exclusion of the contributions from above physical factors may potentially lead to misunderstanding of underlying mechanism and basic physics of nanowires. The large-scale atomistic calculations of nanowires via the PPT used here or the tight-binding approach<sup>51</sup> are of great use in rectifying this situation. Meanwhile, more direct experimental DOS measurements for nanowires are called for to verify the novel DOS features we predicted here.

## AUTHOR INFORMATION

### Corresponding Authors

\*E-mail: ljzhang13@gmail.com.

\*E-mail: alex.zunger@colorado.edu.

### Present Addresses

<sup>§</sup>Key Laboratory of Quantum Information, University of Science and Technology of China, Hefei, Anhui 230026, China.

<sup>||</sup>State Key Laboratory for Superlattices and Microstructures, Institute of Semiconductors, Chinese Academy of Sciences, P.O. Box 912, Beijing 100083, China.

<sup>†</sup>College of Materials Science and Engineering, Jilin University, Changchun 130012, China.

## Notes

The authors declare no competing financial interest.

## ACKNOWLEDGMENTS

Work at CU Boulder by J.W., A.Z., and L.Z. was supported by Office of Science, Basic Energy Science, Materials Sciences and Engineering Division under grant DE-FG02-13ER46959 to CU.

## REFERENCES

- (1) Cui, Y.; Zhong, Z.; Wang, D.; Wang, W. U.; Lieber, C. M. High performance silicon nanowire field effect transistors. *Nano Lett.* **2003**, *3*, 149–152.
- (2) Colinge, J.-P.; Lee, C.-W.; Afzalian, A.; Akhavan, N. D.; Yan, R.; Ferain, I.; Razavi, P.; O'Neill, B.; Blake, A.; et al. Nanowire transistors without junctions. *Nat. Nano* **2010**, *5*, 225–229.
- (3) Duan, X.; Huang, Y.; Agarwal, R.; Lieber, C. M. Single-nanowire electrically driven lasers. *Nature* **2003**, *421*, 241–245.
- (4) Johnson, J. C.; Choi, H.-J.; Knutsen, K. P.; Schaller, R. D.; Yang, P.; Saykally, R. J. Single gallium nitride nanowire lasers. *Nat. Mater.* **2002**, *1*, 106–110.
- (5) Huang, M. H.; Mao, S.; Feick, H.; Yan, H.; Wu, Y.; Kind, H.; Weber, E.; Russo, R.; Yang, P. Room-temperature ultraviolet nanowire nanolasers. *Science* **2001**, *292*, 1897–1899.
- (6) Hochbaum, A. I.; Chen, R.; Delgado, R. D.; Liang, W.; Garnett, E. C.; Najarian, M.; Majumdar, A.; Yang, P. Enhanced thermoelectric performance of rough silicon nanowires. *Nature* **2008**, *451*, 163–167.
- (7) Boukai, A. I.; Bunimovich, Y.; Tahir-Kheli, J.; Yu, J.-K.; Goddard, W. A., III; Heath, J. R. Silicon nanowires as efficient thermoelectric materials. *Nature* **2008**, *451*, 168–171.
- (8) Hu, L.; Chen, G. Analysis of optical absorption in silicon nanowire arrays for photovoltaic applications. *Nano Lett.* **2007**, *7*, 3249–3252.
- (9) Tian, B.; Zheng, X.; Kempa, T. J.; Fang, Y.; Yu, N.; Yu, G.; Huang, J.; Lieber, C. M. Coaxial silicon nanowires as solar cells and nanoelectronic power sources. *Nature* **2007**, *449*, 885–889.
- (10) Kelzenberg, M. D.; Boettcher, S. W.; Petykiewicz, J. A.; Turner-Evans, D. B.; Putnam, M. C.; Warren, E. L.; Spurgeon, J. M.; Briggs, R. M.; Lewis, N. S.; et al. Enhanced absorption and carrier collection in Si wire arrays for photovoltaic applications. *Nat. Mater.* **2010**, *9*, 239–244.
- (11) Law, M.; Greene, L. E.; Johnson, J. C.; Saykally, R.; Yang, P. Nanowire dye-sensitized solar cells. *Nat. Mater.* **2005**, *4*, 455–459.
- (12) Wallentin, J.; Anttu, N.; Asoli, D.; Huffman, M.; Åberg, L.; Magnusson, M. H.; Siefert, G.; Fuss-Kailuweit, P.; Dimroth, F.; et al. InP nanowire array solar cells achieving 13.8% efficiency by exceeding the ray optics limit. *Science* **2013**, *339*, 1057–1060.
- (13) Mourik, V.; Zuo, K.; Frolov, S. M.; Plissard, S. R.; Bakkers, E. P. a. M.; Kouwenhoven, L. P. Signatures of Majorana fermions in hybrid superconductor-semiconductor nanowire devices. *Science* **2012**, *336*, 1003–1007.
- (14) Das, A.; Ronen, Y.; Most, Y.; Oreg, Y.; Heiblum, M.; Shtrikman, H. Zero-bias peaks and splitting in an Al-InAs nanowire topological superconductor as a signature of Majorana fermions. *Nat. Phys.* **2012**, *8*, 887–895.
- (15) Gudiksen, M. S.; Lauhon, L. J.; Wang, J.; Smith, D. C.; Lieber, C. M. Growth of nanowire superlattice structures for nanoscale photonics and electronics. *Nature* **2002**, *415*, 617–620.
- (16) Caroff, P.; Dick, K. A.; Johansson, J.; Messing, M. E.; Deppert, K.; Samuelson, L. Controlled polytypic and twin-plane superlattices in iii–v nanowires. *Nat. Nano* **2009**, *4*, 50–55.

- (17) Ma, D. D. D.; Lee, C. S.; Au, F. C. K.; Tong, S. Y.; Lee, S. T. Small-diameter silicon nanowire surfaces. *Science* **2003**, *299*, 1874–1877.
- (18) Hu, J.; Odom, T. W.; Lieber, C. M. Chemistry and physics in one dimension: synthesis and properties of nanowires and nanotubes. *Acc. Chem. Res.* **1999**, *32*, 435–445.
- (19) Kuykendall, T.; Pauzaskie, P. J.; Zhang, Y.; Goldberger, J.; Sirbuly, D.; Denlinger, J.; Yang, P. Crystallographic alignment of high-density gallium nitride nanowire arrays. *Nat. Mater.* **2004**, *3*, 524–528.
- (20) Halpern, E.; Elias, G.; Kretinin, A. V.; Shtrikman, H.; Rosenwaks, Y. Direct measurement of surface states density and energy distribution in individual InAs nanowires. *Appl. Phys. Lett.* **2012**, *100*, 262105.
- (21) Ford, A. C.; Kumar, S. B.; Kapadia, R.; Guo, J.; Javey, A. Observation of degenerate one-dimensional sub-bands in cylindrical InAs nanowires. *Nano Lett.* **2012**, *12*, 1340–1343.
- (22) Tian, Y.; Sakr, M. R.; Kinder, J. M.; Liang, D.; MacDonald, M. J.; Qiu, R. L. J.; Gao, H.-J.; Gao, X. P. A. One-dimensional quantum confinement effect modulated thermoelectric properties in InAs nanowires. *Nano Lett.* **2012**, *12*, 6492–6497.
- (23) Lundstrom, M., Guo, J., Eds. *Nanoscale Transistors: Device Physics, Modeling and Simulation*; Springer Science & Business Media: New York, 2006.
- (24) Shah, J., Ed. *Hot Carriers in Semiconductor Nanostructures: Physics and Applications*, 1st ed.; Academic Press: Boston, MA, 1992.
- (25) Harrison, P., Ed. *Quantum Wells, Wires and Dots: Theoretical and Computational Physics of Semiconductor Nanostructures*, 3rd ed.; Wiley: West Sussex, U.K., 2010.
- (26) Wang, L. W.; Zunger, A. Electronic structure pseudopotential calculations of large (~1000 Atoms) Si quantum dots. *J. Phys. Chem.* **1994**, *98*, 2158–2165.
- (27) Canning, A.; Wang, L. W.; Williamson, A.; Zunger, A. Parallel empirical pseudopotential electronic structure calculations for million atom systems. *J. Comput. Phys.* **2000**, *160*, 29–41.
- (28) Zunger, A. Pseudopotential theory of semiconductor quantum dots. *Phys. Status Solidi B* **2001**, *224*, 727–734.
- (29) Fu, H.; Wang, L.-W.; Zunger, A. Comparison of the  $k\cdot p$  and the direct diagonalization approaches for describing the electronic structure of quantum dots. *Appl. Phys. Lett.* **1997**, *71*, 3433–3435.
- (30) Fu, H.; Wang, L.-W.; Zunger, A. Applicability of the  $k\cdot p$  method to the electronic structure of quantum dots. *Phys. Rev. B* **1998**, *57*, 9971–9987.
- (31) An, J. M.; Franceschetti, A.; Dudy, S. V.; Zunger, A. The peculiar electronic structure of PbSe quantum dots. *Nano Lett.* **2006**, *6*, 2728–2735.
- (32) Wang; Zunger, A. High-energy excitonic transitions in CdSe quantum dots. *J. Phys. Chem. B* **1998**, *102*, 6449–6454.
- (33) Bester, G.; Zunger, A. Cylindrically shaped zinc-blende semiconductor quantum dots do not have cylindrical symmetry: Atomistic symmetry, atomic relaxation, and piezoelectric effects. *Phys. Rev. B* **2005**, *71*, 045318.
- (34) Zhang, L.; Luo, J.-W.; Zunger, A.; Akopian, N.; Zwiller, V.; Harmand, J.-C. Wide InP nanowires with wurtzite/zincblende superlattice segments are type-II whereas narrower nanowires become type-I: an atomistic pseudopotential calculation. *Nano Lett.* **2010**, *10*, 4055–4060.
- (35) Zhang, L.; Luo, J.-W.; Franceschetti, A.; Zunger, A. Excitons and excitonic fine structures in Si nanowires: prediction of an electronic state crossover with diameter changes. *Phys. Rev. B* **2011**, *84*, 075404.
- (36) Zhang, L.; D’Avezac, M.; Luo, J.-W.; Zunger, A. Genomic design of strong direct-gap optical transition in Si/Ge core/multishell nanowires. *Nano Lett.* **2012**, *12*, 984–991.
- (37) Duan, X.; Lieber, C. M. General synthesis of compound semiconductor nanowires. *Adv. Mater.* **2000**, *12*, 298–302.
- (38) BenDaniel, D. J.; Duke, C. B. Space-charge effects on electron tunneling. *Phys. Rev.* **1966**, *152*, 683–692.
- (39) Yu, P., Cardona, M., Eds. *Fundamentals of Semiconductors: Physics and Materials Properties*; Springer: New York, 2010.
- (40) Rama Krishna, M. V.; Friesner, R. A. Exciton spectra of semiconductor clusters. *Phys. Rev. Lett.* **1991**, *67*, 629–632.
- (41) Zhang, S. B.; Yeh, C.-Y.; Zunger, A. Electronic structure of semiconductor quantum films. *Phys. Rev. B* **1993**, *48*, 11204–11219.
- (42) Franceschetti, A.; Zunger, A. GaAs quantum structures: Comparison between direct pseudopotential and single-band truncated-crystal calculations. *J. Chem. Phys.* **1996**, *104*, 5572–5578.
- (43) Cohen, M. L.; Bergstresser, T. K. Band structures and pseudopotential form factors for fourteen semiconductors of the diamond and zinc-blende structures. *Phys. Rev.* **1966**, *141*, 789–796.
- (44) Wang, L.-W.; Kim, J.; Zunger, A. Electronic structures of [110]-faceted self-assembled pyramidal InAs/GaAs quantum dots. *Phys. Rev. B* **1999**, *59*, 5678–5687.
- (45) Wang, L.; Zunger, A. Solving Schrödinger’s equation around a desired energy: Application to silicon quantum dots. *J. Chem. Phys.* **1994**, *100*, 2394–2397.
- (46) Efros, A. L.; Rosen, M. Quantum size level structure of narrow-gap semiconductor nanocrystals: Effect of band coupling. *Phys. Rev. B* **1998**, *58*, 7120–7135.
- (47) Sercel, P. C.; Vahala, K. J. Analytical formalism for determining quantum-wire and quantum-dot band structure in the multiband envelope-function approximation. *Phys. Rev. B* **1990**, *42*, 3690–3710.
- (48) Cardona, M. Electron effective masses of InAs and GaAs as a function of temperature and doping. *Phys. Rev.* **1961**, *121*, 752–758.
- (49) Wang, L.-W.; Bellaiche, L.; Wei, S.-H.; Zunger, A. Majority representation of alloy electronic states. *Phys. Rev. Lett.* **1998**, *80*, 4725–4728.
- (50) Thelander, C.; Agarwal, P.; Brongersma, S.; Eymery, J.; Feiner, L. F.; Forchel, A.; Scheffler, M.; Riess, W.; Ohlsson, B. J.; et al. Nanowire-based one-dimensional electronics. *Mater. Today* **2006**, *9*, 28–35.
- (51) Luisier, M.; Schenk, A.; Fichtner, W.; Klimeck, G. Atomistic simulation of nanowires in the  $sp^3d^5s^*$  tight-binding formalism: from boundary conditions to strain calculations. *Phys. Rev. B* **2006**, *74*, 205323.